

1 **Tracing the second stage of Antarctic ozone hole recovery with a “big data”**

2 **approach to multi-variate regressions**

3

4 A.T.J. de Laat, R.J. van der A, M. van Weele

5

6 Royal Netherlands Meteorological Institute, De Bilt, The Netherlands.

7

8

9 **Abstract**

10

11 This study presents a sensitivity analysis of multi-variate regressions of recent
12 springtime Antarctic vortex ozone trends using a “big data” ensemble approach.

13 Our results indicate that the poleward heat flux (Eliassen-Palm Flux) and the effective
14 chlorine loading explain, respectively, most of the short-term and long-term variability in
15 different Antarctic springtime total ozone records. The inclusion in the regression of
16 stratospheric volcanic aerosols, solar variability and the Quasi-Biennial Oscillation is
17 shown to increase rather than to decrease the overall uncertainty in the attribution of
18 Antarctic springtime ozone because of large uncertainties in their respective records.

19 Calculating the trend significance for the ozone record from the late 1990s onwards
20 solely based on the fit of the effective chlorine loading is not recommended, as this does
21 not take fit residuals into account resulting in too narrow uncertainty intervals, while the
22 fixed temporal change of the effective chlorine loading does not allow for any flexibility
23 in the trends.

24 When taking fit residuals into account into a piecewise linear trend fit, we find that
25 approximately 30-60% of the regressions in the full ensemble result in a statistically
26 significant positive springtime ozone trend over Antarctica from the late 1990s onwards.
27 Analysis of choices and uncertainties in time series show that, depending on choices in
28 time series and parameters, the fraction of statistically significant trends in parts of the
29 ensemble can range from negligible to a complete 100%. We also find that, consistent
30 with expectations, the number of statistically significant trends increases with increasing
31 record length.

32 Although our results indicate that the use multivariate regressions is a valid approach
33 for assessing the state of Antarctic ozone hole recovery, and it can be expected with
34 increasing record length results will move towards more confidence in recovery,
35 uncertainties in choices currently do not yet support formal identification of recovery of
36 the Antarctic Ozone Hole.

37

38 **1. Introduction**

39

40 An important question in 21st century ozone research is whether the ozone layer is
41 starting to recover as a result of the measures taken to reduce emissions of Ozone
42 Depleting Substances (ODS) as agreed on in the Montreal Protocol [UNEP, 2012] and its
43 subsequent amendments and adjustments.

44 The World Meteorological Organization has defined three different stages of ozone
45 recovery [WMO, 2007]. The first stage consists of a slowing of ozone depletion,
46 identified as the occurrence of a statistically significant reduction in the rate of decline in
47 ozone due to changing stratospheric halogens. The second stage revolves around the
48 onset of ozone increase (turnaround), identified as *the occurrence of statistically*
49 *significant increases in ozone - above a previous minimum value - that can be attributed*
50 *to declining stratospheric halogens*. Note that what is meant by “statistically significant”
51 is not specified. Finally, the third stage is the full recovery of ozone from ODSs,
52 identified as when the ozone layer is no longer affected by ODSs, or alternatively, once
53 stratospheric ozone levels have returned to pre-1980 values.

54 The first stage of ozone recovery has already been identified in observations to have
55 occurred roughly in the late 1990s [WMO 2007, 2011]. The third stage is not expected to
56 occur until somewhere halfway the 21st century or later [WMO, 2011]. The spatial
57 distribution of total ozone after the third stage probably differs somewhat from the pre-
58 1980 distribution due to climate change – in particular changes in the stratospheric
59 chemical composition and temperature structure [Bekki et al., 2011, and references
60 therein].

61 As far as the second stage of ozone recovery is concerned, it has recently been argued
62 that a statistically significant increase in ozone beyond a minimum and attributable to
63 decreases in ODSs can be identified for the Antarctic ozone hole [Salby et al., 2011,
64 2012; Kuttippurath et al., 2013; Knibbe et al, 2014]. To some extent this is surprising as it
65 has long been thought that identification of the second stage of ozone recovery could only
66 be expected after 2020 [*e.g.* Newman et al., 2006; Eyring et al., 2007]. Those estimates
67 were based on (model) simulations of ozone from which it is calculated when the ozone
68 trend from a certain starting year onwards would qualify for “statistically significant”, or
69 in other words, would emerge from the year-to-year natural variations in ozone (“noise”).
70 Such methods implicitly assume that ozone variations around the trend are not
71 deterministic (random).

72 However, it has also long been established that many stratospheric ozone variations are
73 in fact deterministic. Various processes have been identified that affect stratospheric
74 ozone variability in the Southern Hemisphere on an inter-annual basis, like volcanic
75 aerosols [Telford et al., 2009], the Southern Annular Mode (SAM) [Thompson and
76 Wallace, 2000; Jiang et al., 2008], the poleward heat flux or Eliassen-Palm flux (EP flux)
77 [Randel et al., 2002], solar variability [Soukharev and Hood, 2006], and the Quasi
78 Biennial Oscillation (QBO) [Jiang et al., 2008]. If the physics and chemistry are
79 sufficiently understood, it might be possible to filter out part of the ozone variations from
80 the ozone records by means of a multi-variety regression, resulting in a smoother ozone
81 record for which trend significance might be reached earlier. This approach, in essence,
82 forms the basis of the suggested identification of the second stage of ozone recovery
83 reported by Salby et al. [2011, 2012], Kuttippurath et al. [2013] and Knibbe et al [2014].

84 However, none of these studies did systematically consider the uncertainties in the
85 proxies that were selected for the regressions. In addition, no motivation or discussion
86 was provided for the choice of a specific ozone record, *e.g.* a consideration of taking
87 annual, seasonal, and/or monthly means of total ozone, and the integration over a chosen
88 spatial domain.

89 Hence, we want to address the following question in this study: Is the suggested
90 detection of the second stage of ozone recovery robust when uncertainties in the
91 regression parameters and for different selected ozone records are taken into account?
92 This question is approached here with combined multiple scenario – Monte Carlo
93 ensemble simulations using the same regression methodology as presented in
94 Kuttippurath et al. [2013] but by inclusion of various uncertainties leading to a large
95 ensemble of different regressions. We analyze this “big data” ensemble for robustness of
96 the individual regressions.

97 Kuttippurath et al. [2013] considered different Antarctic vortex definitions and thus
98 different vortex ozone records. They found that regression results were not very sensitive
99 to the Antarctic vortex definition. Hence, we decided to use September-November
100 Antarctic vortex core (poleward of 70°S) average total ozone column based on the Multi
101 Sensor Reanalysis (MSR; van der A et al. [2010]), also because from a practical point of
102 view this definition does not require additional information about the location of the
103 vortex edge. The selected regressors are the SAM, solar flux, QBO, EP flux, stratospheric
104 volcanic aerosols and the Equivalent Effective Stratospheric Chlorine (EESC), similar to
105 Kuttippurath et al. [2013]. The EESC can be used to estimate ozone trends. Kuttippurath
106 et al. [2013] also calculated Piece Wise Linear Trends (PWLT) for estimating ozone

107 trends as alternative for the EESC-based ozone trends, an approach we will follow here as
108 well.

109 In this paper, we extend the analysis by introducing both several differing scenarios for
110 the ozone record and regressor records of the EP flux, volcanic aerosols, and EESC.
111 Monte Carlo variations were applied to the regressor records of the solar flux, QBO,
112 SAM by adding random variations. While we focus on parameter uncertainties in this
113 study, additional uncertainties do exist, for example with respect to possible time lags
114 between regressors and the ozone record. The resulting ensemble of regression results
115 provides a big data pool of about 23 million different regressions that is analyzed in terms
116 of probability distributions of the explanatory power of the regressions (R^2), the ozone
117 trends and corresponding ozone trend uncertainties, and the regression coefficient values
118 quantifying the dependence of ozone on a particular regressor. We also investigate if
119 some way of optimization is possible for the chosen scenarios, and we discuss the
120 likelihood of detection of the second stage of ozone recovery within the context of all
121 uncertainties presented. Note that the uncertainties discussed here differ from formal
122 errors that come with a standard multi-variate regression. Also note that we implicitly
123 assume that the relation between the independent variables and ozone is linear, even
124 though the relation may very well be non-linear. The latter will to some extent be
125 considered in our study and is part of the discussion of the results, but the issue of non-
126 linearity of the regressor-ozone relation is not addressed in detail, in particular because,
127 as will be shown, for many regressors the non-linearity of its relation with ozone is
128 insufficiently characterized, or even unknown.

129 This paper is organized as follows. Section 2 describes the observational datasets used
130 and the ozone and regressor scenarios or Monte Carlo simulations performed. Section 3
131 discusses the probability distributions of the explanatory power of the regressions, trends
132 and regression values, including how the distributions depend on scenarios or Monte
133 Carlo results. Section 4 discusses the question of detection of the second stage of ozone
134 recovery, and in section 5 everything is wrapped up and some conclusions are drawn.

135

136 **2. Multivariate regression parameter uncertainties**

137

138 Online data sources of the ozone observation records and applied regressors can be
139 found in Table 1.

140

141 **2.1 Method**

142

143 A common method for analyzing total ozone records is the use of a multi-variate linear
144 regression, a method that we will use in this paper as well. The goal of the method is to
145 attribute both inter-annual as well as decadal variations in the ozone record to processes
146 that are expected or known to affect the total ozone record (Kuttippurath et al. [2013],
147 and references therein). In the regression, the total ozone variability (Y) as a function of
148 time (t) is expressed as

149

150 $Y(t) = K$ (Constant)

151 $+ C_{JHF}(t)$ (Poleward Heat Flux or Eliassen-Palm (EP) flux)

152 + $C_2\text{SAM}(t)$ (Southern Annual Mode index)
153 + $C_3(\text{SF} \times \text{QBO})(t)$ (Solar Flux \times QBO index)
154 + $C_4\text{Aer}(t)$ (Stratospheric Aerosol optical depth)
155 + $C_5\text{Trend}(t)$ (Total ozone trend)
156 + $\varepsilon(t)$ (Total ozone residual)

157

158 In which t is the time from 1979 to 2010 or 2012, K is a constant and regression
159 coefficients C_1 to C_5 are the regression coefficients for the respective proxies. The ozone
160 trend (C_5) can be related to the time-dependent equivalent effective stratospheric chlorine
161 loading (EESC) or a piecewise linear trend (PWLT) before and after a predefined break
162 year. The PWLT regressions are calculated by including two linear terms in the
163 regression: the first term is a linear fit for the entire time window, the second term is a
164 linear term only for the years after a chosen break year [Kuttippurath et al., 2013].

165 The analysis of regression results will focus on two parameters that have previously
166 been used in papers investigating Antarctic ozone recovery [Yang et al., 2008; Salby et
167 al., 2011, 2012; Kuttippurath et al., 2013; Knibbe et al., 2014]: the serial correlation R
168 between the regression-based ‘reconstructed’ ozone record and the observations, and the
169 post-break trends and trend significance. Since the focus of our paper is to investigate
170 trend significance, not specifically what parameters can best explain Antarctic ozone, we
171 will only look in some detail at the usefulness of certain regressors. However, our
172 analysis does provide indications of what are more and less useful regressors.

173 In sections 2.2 to 2.7 the uncertainty in each of the proxies that is used as a regressor is
174 discussed. These uncertainty ranges determine the spread in the ensemble that is used in

175 the “big data” analysis. A summary of the regressor uncertainties and how they are
176 incorporated in this study can be found in Table 2. The solar flux and QBO are combined
177 into one proxy as discussed in section 2.3.

178

179 **2.2 Poleward heat flux (EP flux)**

180

181 Figure 1 shows the poleward heat flux, here represented by the (vertical) EP flux
182 [Andrews et al., 1987] at the 70-hPa level and averaged poleward of 40°S for the
183 combined months of August and September, as well as the average EP flux available for
184 a given year for a variety of datasets. Note that the datasets do not all completely overlap
185 in time. Before 2000 there are considerable differences between the datasets. After 2000
186 these differences are smaller, which to some extent is traced to the lack of ERA40 data
187 beyond 2001 and lack of JRA data beyond 2004. The lower panel shows the relative
188 differences between the five datasets and their mean. The standard deviation of all data is
189 7.65%, but from 2000 onwards only 2.67%.

190 Another source of uncertainty in the use of the EP flux as proxy is the choice of the
191 time window over which the average EP flux is calculated. This choice depends on what
192 is thought to be the relationship between variations in EP flux and ozone depletion. The
193 basic theory states that the poleward movement of stratospheric air is proportional to the
194 strength of the residual mean stratospheric circulation (Brewer-Dobson circulation),
195 which in turn is driven by the poleward eddy heat flux. The poleward eddy heat flux is
196 expressed by the upward component of the Eliassen-Palm flux that measures the upward
197 transport of momentum by planetary waves [Andrews et al., 1987; Salby et al., 2012, and

198 references therein]. Planetary wave activity in the Northern Hemisphere affects Arctic
199 Polar vortex stability and thus Arctic ozone depletion. However, to what extent this is
200 similar in the Southern Hemisphere is still a topic of debate. The Arctic and Antarctic
201 may behave either similarly [Weber et al., 2003; 2011] or not [Salby et al., 2012]. This is
202 because the notion of hemispheric similarities in how the EP flux affects ozone depletion
203 so far is heavily based on only one outlier year (2002 for the SH, 2011 for the NH).

204 Current research efforts try to gain a better understanding of the physical and
205 photochemical mechanisms by which the heat flux and planetary wave action affects
206 Antarctic stratospheric ozone. A recently proposed mechanism [de Laat and van Weele,
207 2011] involves a pre-conditioning of Antarctic inner stratospheric vortex air whereby
208 stratospheric temperatures affect PSC formation which in turn affects the buildup of a
209 halogen reservoir that later during Austral spring changes the rate of catalytic ozone
210 destruction. This preconditioning mechanism explains some years with anomalous ozone
211 depletion, but not all. For example, during Austral winter 2013 the Antarctic vortex
212 remained largely undisturbed – opposite to 2010 and 2012, see de Laat and van Weele
213 [2011] and Klekociuck et al. [2011], thus allowing for widespread PSC formation and
214 pre-conditioning the inner vortex air for efficient ozone depletion. However, from the
215 start of Austral spring 2013 (halfway August) onwards the Antarctic stratospheric vortex
216 got disturbed by planetary wave activity. As a result, the amount of springtime ozone
217 depletion remained below what has been experienced during previous years with similar
218 preconditioning. This suggests that there are multiple pathways as well as complicated
219 interactions between chemistry and physics that can lead to reduced Antarctic springtime

220 ozone depletion. Hence, it is unclear which regressor or regressors could act as proxies
221 for these complex processes.

222 A further complicating factor is the disintegration of the Antarctic vortex, which is
223 again controlled by planetary wave activity [Kramarova et al., 2014]. The stability of the
224 vortex determines how long the ozone depleted inner-vortex air remains intact after
225 photochemical ozone depletion ceases during Austral spring. Variations in the duration of
226 Antarctic vortex stability introduce variations in the Antarctic total ozone record which
227 are not related to variations in photochemistry.

228 We attempt to reflect these issues in our uncertainty range for the proxy used to account
229 for the EP flux variations in multivariate regressions. Salby et al. [2011, 2012] and
230 Kuttippurath et al. [2013] use the August – September mean EP flux poleward of 40°S
231 and at the 70-hPa level, the baseline also used in this study. Weber et al. [2011] uses the
232 100-hPa poleward heat flux rather than the 70-hPa heat flux and the average over the
233 region between 45°S and 75°S rather than between 40°S and 90°S. They further show that
234 there is no particular favorable wintertime month or period from the perspective of
235 Antarctic springtime ozone depletion over which to average the EP flux. Hence there is a
236 certain arbitrariness involved in selecting the optimum EP flux averaging period and
237 region.

238 For our study we define eight different EP flux scenarios, using different periods,
239 latitudes and heights (see Table 2), all based on the ECMWF ERA Interim dataset.
240 Performing the same exercise as in Figure 1 for these eight scenarios, the standard
241 deviation of the EP flux time series is 21.5%. This is considerably larger than the
242 variability among the same EP fluxes of the different reanalysis datasets discussed above.

243 Thus, the uncertainty in EP flux estimates largely originates in using different periods,
244 latitudes and/or heights for which the EP flux is calculated, rather than in the use of
245 different reanalysis datasets to calculate the same EP flux.

246

247

248 **2.3 The mixed solar-QBO index**

249

250 In Kuttippurath et al. [2013] the effects of solar variability and QBO variability are
251 combined into one proxy. As explained in Holton and Tan [1990], in studying high-
252 latitude variability and trends the QBO and solar effects cannot be considered separately.
253 Whereas the solar influence modifies tropical stratospheric ozone and dynamics, the
254 transport of the solar signal to higher/polar latitudes depends on the phase of the QBO.
255 As a result, solar effects on winter polar Antarctic stratospheric temperatures also depend
256 on the phase of the QBO [Labitzke, 2004]. If the QBO is westerly (easterly), stratospheric
257 temperatures vary in phase (out of phase) with solar activity. It has been proposed by
258 Haigh and Roscoe [2006] and Roscoe and Haigh [2007] to combine the QBO and solar
259 activity into a new regression index that takes this effect into account:

$$260 \quad \text{Solar} - \text{QBO index} = (\text{Solar} - S_m) \times (\text{QBO} - Q_m)$$

261 In which S_m is the mean of the solar flux and Q_m the midpoint of the QBO range.
262 However, as Roscoe and Haigh [2007] note, this new index is rather sensitive to the
263 choice of S_m and Q_m , in particular as the index is by construction the product of two
264 anomaly fields, and thus sensitive to sign changes. In addition, the choice of S_m and Q_m is
265 also arbitrary. Roscoe and Haigh [2007] solve this by selecting averages for which the

266 best total ozone column regression results are obtained. However, the best regression
267 results may not necessarily mean that the regressor is the best representation of the
268 underlying physical mechanism, in particular as regression results also depend on other
269 proxies and in principle there can be a cancellation of errors from different proxies in the
270 regression. Thus, the sensitivity of the combined solar-QBO index on the calculation
271 method of the anomalies must be further investigated.

272 Figure 2 shows the resulting solar flux – QBO index time series, given various
273 assumptions in its calculation. Clearly there is a considerable variability in the index
274 values. The lower plot shows that the variability for every single anomaly varies by \pm
275 200%. This is rather large compared to the estimated uncertainties in both individual
276 solar flux and QBO proxies. Hence, using a combined solar flux – QBO proxy introduces
277 a considerable amount of additional uncertainty. For the uncertainty range in our
278 regressions we construct 100 Monte Carlo time series in which for each single solar-flux
279 QBO index value random Gaussian noise is added with an amplitude of 200% of the
280 index value.

281 Note that the uncertainties in the individual QBO and solar flux proxies are much
282 smaller than the uncertainty in the combined solar flux – QBO index which is relevant for
283 high-latitude trends (see supplementary information for a separate discussion of the solar
284 flux and QBO index).

285

286 **2.4 Southern Annular Mode**

287

288 The Southern Annular Mode (SAM) is a widely used index that reflects the zonal
289 symmetry of the tropospheric circulation in the Southern Hemisphere. The symmetry of
290 the Southern Hemisphere circulation has long been identified as an important mode of
291 variability of the Southern Hemisphere climate. A positive index is characterized by
292 anomalously high surface pressure at mid-latitudes and anomalously low surface pressure
293 at latitudes closer to Antarctica.

294 The SAM used in this study is derived from the National Oceanic and Atmospheric
295 Administration (NOAA). It is based on Empirical Orthogonal Functions (EOF) applied to
296 the monthly mean National Centers for Environmental Prediction and National Center for
297 Atmospheric Research (NCEP/NCAR) reanalysis [Kalnay et al., 1996] 700-hPa height
298 anomalies poleward of 20°S for the Southern Hemisphere, with the seasonal cycle being
299 removed. The monthly SAM index is constructed by projecting the daily and monthly
300 mean 700-hPa height anomalies onto the leading EOF mode. Both time series are
301 normalized by the standard deviation of the monthly index (1979-2000 base time period).
302 Since the leading pattern of SAM is obtained using the monthly mean height anomaly
303 dataset, the index corresponding to each loading pattern becomes one when it is
304 normalized by the standard deviation of the monthly index.

305 However, there is no unique SAM index due to the existence of different
306 meteorological datasets and different methods to quantify the symmetry of the Southern
307 Hemisphere circulation. Kuttippurath et al. [2013] use the AntArctic Oscillation (AAO)
308 index, which is in fact a certain choice of SAM index. A study by Ho et al. [2012]
309 provides a comprehensive analysis of eight different SAM indices. Their analysis shows
310 that the correlation (R^2) between the indices varies between 0.45 and 0.96 for seasonal

311 values and 0.73 and 0.96 for monthly values. This corresponds with random (Gaussian)
312 variations between 20-100% (root-mean-square value). For most of the indices the
313 correlation is better than 0.75. As a point of reference, adding random Gaussian noise of
314 50% to a time series of a parameter and calculating its correlation with the original time
315 series results to a correlation (R^2) of almost 0.8.

316 For the uncertainty analysis we construct 100 Monte Carlo time series in which for each
317 single SAM index value Gaussian noise is added with – to be on the conservative side -
318 an amplitude of 100% of the index value.

319

320 **2.5 EESC loading**

321

322 Uncertainties in the estimates of the EESC loading originate from two factors: the mean
323 age-of-air, which reflects how fast stratospheric halogen concentrations decline due to
324 transport velocity of halogen poor tropospheric air from the tropical stratosphere to the
325 polar stratosphere, and the so-called ‘fractional release’, the rate with which Ozone
326 Depleting Substances (ODSs) release chlorine and bromine in the stratosphere. ODSs
327 typically have not yet been dissociated when they enter the stratosphere at the tropical
328 tropopause, and thus have fractional release values of zero. After transiting through the
329 upper stratosphere, the ODSs in an air parcel get fully dissociated due to their exposure to
330 energetic radiation and the fractional release values get close to 1.0 [Newman et al.,
331 2007].

332 To complicate matters, the mean age-of-air in the stratosphere is not a constant but
333 varies with latitude, height and season [Stiller et al., 2008]. On average, the age-of-air

334 increases with height, *i.e.* it takes longer for tropospheric air to travel higher in the
335 stratosphere, and the age-of-air also increases towards the poles because of the time it
336 takes for air to travel from the tropical “source” region to higher latitudes. In the
337 Antarctic vortex regions there is a strong seasonal dependence of the age-of-air due to the
338 isolation of inner vortex air during Austral winter and spring, while upper stratospheric
339 and mesospheric air slowly descends in the Antarctic vortex. The descending air is
340 particularly “old” air and causes strong vertical gradients in the age-of air in the
341 wintertime polar vortex. Stiller et al. [2008; their figure 7] show that the age-of-air almost
342 triples going up from 15 km ($\theta = 400$ K; age-of-air ~ 4 years), to 20 km ($\theta = 400$ K; age-
343 of air ~ 7 years), to 25 km ($\theta = 600$ K; age-of-air ~ 9 years), to finally 30 km ($\theta = 750$ K;
344 age-of-air ~ 11 years). How to account for this variability in a regression is unclear, but it
345 is unlikely that one age-of-air value can be attributed to the total ozone column.

346 Moreover, ozone variability in the Antarctic vortex is determined by different processes
347 at different altitudes. Halogen related ozone depletion typically maximizes between 15-20
348 km altitude (~ 100 -50 hPa, US Standard atmosphere 1976; $\theta = 400$ -500 K), whereas the
349 effect of vortex stability on ozone depletion is seen predominantly between 20-30 km
350 altitude (~ 50 -10 hPa; $\theta = 500$ -750 K) [de Laat and van Weele, 2011]. Thus, total ozone
351 columns observations which are vertically integrated amounts of ozone are being affected
352 by different processes at different altitudes.

353 The age-of-air may also not be constant over the time period over which ozone trends
354 are determined. Due to a changing climate the stratospheric circulation may speed up
355 [*e.g.* Engel et al., 2009; Bunzel and Schmidt, 2013], causing a decrease in the age-of-air
356 with increased warming, which obviously then depends on the exact warming. This

357 introduces yet another uncertainty for the periods from 1979 to 2010 or 2012 that are
358 considered in this study.

359 The age-of-air uncertainties do not manifest themselves as a random process, which
360 would make it useful for applying a Monte Carlo method, but as a structural uncertainty,
361 *i.e.* the entire EESC shape would change for different parameter settings. Such
362 uncertainty could be captured by applying a parametric bootstrap rather than a Monte
363 Carlo approach. However, such parametric approach would also not suffice because we
364 use total column observations and we know that ozone at different altitudes would be
365 affected by different parameter values.

366 A pragmatic approach with regard to the sensitivity of the regression to EESC values is
367 testing the robustness of the regression results as a function of the assumed EESC time
368 evolution. For the uncertainty analysis we assume three different EESC scenarios with an
369 age-of-air of 2.5, 4 and 5.5 years and a half-width of, respectively, 1.25, 2 and 2.75 years.
370 Largest differences between the three scenarios are in their post-peak trend in EESC (see
371 later on in Figure 3).

372

373 **2.6 Volcanic aerosol.**

374

375 Aerosols from sufficiently strong volcanic eruptions can reach the stratosphere and
376 affect stratospheric ozone chemistry. In particular strong eruptions occurring in the
377 tropics can have long lasting effects on stratospheric ozone. Aerosols reaching the
378 tropical stratosphere are slowly transported towards middle and high latitudes. It can take
379 up to a decade before the stratosphere is cleared from volcanic aerosols [Vernier et al.

380 2011; Solomon et al., 2011]. Volcanic eruptions at middle and high latitudes have much
381 shorter lasting effects. These aerosols enter in the descending branch of the stratospheric
382 circulation and will be relatively quickly removed from the stratosphere.

383 The short-term effect of stratospheric volcanic aerosols is heating of the stratospheric
384 layer which affects stratospheric ozone in the tropical belt. The dominant long-term effect
385 of stratospheric volcanic aerosols on global and polar ozone is however the increase in
386 aerosol surface area density and subsequent heterogeneous ozone loss. Model simulations
387 of volcanic aerosol effects on stratospheric ozone suggest that in particular under cold
388 conditions (high latitude, wintertime, lower stratosphere) total ozone columns can be
389 reduced by up to 10-15 % [Rozanov et al., 2002]. During other seasons, total ozone
390 column depletion by volcanic aerosols is of the order of a few percent.

391 Since 1979 two major tropical volcanic eruptions have affected stratospheric ozone: El
392 Chichón, Mexico, in 1982, and Pinatubo, Philippines, in 1991. Although the total amount
393 of stratospheric aerosols by both eruptions has been characterized relatively well, there
394 appear to be considerable uncertainties associated with the time evolution of the aerosol
395 amounts in the Southern Hemisphere. A brief and incomplete survey of a latitudinal
396 volcanic aerosol radiative forcing data [Ammann et al., 2003] and a global volcanic
397 aerosol proxy record [Crowley and Unterman, 2012] as well as the standard volcanic
398 aerosol index used in Kuttippurath et al. [2013] – aerosol optical depth, Sato et al. [1993]
399 and updates, available via NASA GISS – all show that there are large differences
400 between the El Chichón aerosol peak relative to the Pinatubo peak. Large differences are
401 seen in global, hemispheric and Southern Hemisphere (Antarctic) aerosol amounts as
402 well as differences in the exact timing of the peak aerosols [Sato et al., 1993; Ammann et

403 al., 2003]; Crowley and Unterman, 2012]. The El Chichón aerosol peak relative to the
404 Pinatubo peak for high Antarctic latitudes can be similar [Ammann et al., 2003], about
405 three times smaller [Sato et al., 1993] to (globally) eight times smaller [Crowley and
406 Unterman, 2012]. The Pinatubo peak aerosol in the Southern Hemisphere was about half
407 the size of the global-mean Pinatubo peak [Ammann et al., 2003].

408 Kuttippurath et al. [2013] shift the Southern Hemisphere aerosol data by six months to
409 account for the transport of aerosols. Although they report that the six month shift results
410 in the best statistics, the analysis presented in the previous paragraph shows that the effect
411 of the shift is relevant for the shape of the volcanic aerosol changes, but does not
412 introduce variations as large as the other variations in volcanic aerosol indices. Given that
413 a time shift is included in the 6 volcanic aerosol scenarios defined above, we do not add
414 additional time shifts in the aerosol record.

415 We define six volcanic aerosol scenarios that reflect the uncertainty in the volcanic
416 stratospheric aerosol records. Base scenario is the scenario used in Kuttippurath et al.
417 [2013] which in turn uses the NASA GISS stratospheric aerosol record. A second
418 scenario is with the Pinatubo aerosol curve scaled so that the maximum matches the El
419 Chichón aerosol peak, the Pinatubo curve maximum is 2.5 times the El Chichón peak,
420 and the Pinatubo curve maximum is five times the El Chichón peak. The uncertainty in
421 timing of the Southern Hemispheric aerosol peak is considered by a shift of the El
422 Chichón peak one year back compared to the Pinatubo peak and a shift of the Pinatubo
423 peak one year back compared to El Chichón peak.

424

425 **2.7 Ozone Scenarios.**

426

427 It is *a priori* unclear what would be the most appropriate ozone scenario to use in the
428 regression. Both Salby et al. [2011, 2012] and Kuttippurath et al. [2013] use the
429 September-November three-month averaged total ozone record. However, as discussed in
430 the introduction, different processes affect ozone during different time periods. Studies in
431 the literature use very different time periods for averaging ozone to investigate Antarctic
432 ozone trends. We define eight different ozone scenarios to reflect the ozone records used
433 in literature (see also de Laat and van Weele [2011]), using the MSR dataset [van der A
434 et al., 2010]. The MSR is a 30-year total O₃ column assimilation dataset for 1979–2008
435 based on a total of eleven satellite instruments measuring total O₃ columns – including
436 SCIAMACHY - that were operating during various periods within these 30 years For the
437 period 2009-2012 the MSR dataset was extended with assimilated SCIAMACHY and
438 GOME-2 total ozone column data. Apart from the September-November three-month
439 averaged total ozone record we also use averages of total ozone over the month of
440 September, the month of October, the two-month period September-October, a very long
441 period (19 July – 1 December), a very short 10-day period (21 – 30 September), the
442 period 7 September – 13 October, and a year-dependent “worst” 30-day period (30-day
443 average with the largest Ozone Mass Deficit).

444

445 **2.8 Other uncertainties**

446

447 Kuttippurath et al. [2013] address two other important uncertainties for the
448 determination of the ozone trend. First, the area over which the ozone record is defined

449 (Inside Vortex, Equivalent Latitude 65°S-90°S, and Vortex Core). The area is important
450 for the absolute amounts of ozone depletion but Kuttippurath et al. [2013] show it is
451 much less relevant for the differences in trend. That is, the uncertainties in the estimated
452 linear trend dominate the uncertainties due to different areas over which the ozone
453 anomalies are calculated. A second uncertainty on their ozone trend derives from the use
454 of different ozone datasets (ground-based, TOMS/OMI and MSR). Also here the
455 uncertainties in the estimated linear trend dominate the uncertainties due to the different
456 data sets. Hence, we do not include these uncertainties in our analysis.

457 In addition, there are many studies trying to identify the moment where ODSs stop
458 increasing and/or where ozone stops decreasing. The maximum ODSs appears
459 somewhere between 1997 and 2000 (Newman et al., 2007), depending on geographical
460 location and height. However, due to saturation effects – there are more than sufficient
461 ODS present to destroy all Antarctic ozone – the moment where ozone starts to be
462 affected by decreasing ODSs may actually be later (Kuttippurath et al., 2013; Kramarova
463 et al., 2014).

464 The moment of a structural break in ozone based on observations indicates an early
465 break around 1997 (Newchurch et al., 2003; Yang et al., 2008). However, some processes
466 affecting stratospheric ozone vary on long time scales – solar effects and volcanic
467 eruptions come to mind – which may affect the observations-based analysis of break
468 points (Dameris et al., 2006). Note that we confirm this break year of 1997 based on a
469 applying a break-point analysis algorithm to the MSR ozone record (not shown). Hence,
470 we decided to use three different break years that have been identified and/or are most
471 commonly used: 1997, 1998 and 1999.

472

473 **2.9 Selected uncertainties ranges and ozone record scenarios.**

474

475 Figure 3 shows the baseline regressor time series and the scenarios for ozone, the EP flux,
476 EESC loading and volcanic aerosols. A total of 100 different solar flux – QBO index and
477 SAM index time series are used to span their uncertainty range (not shown in Figure 3).
478 All scenarios and Monte Carlo results combined provide 11.5 million different choices
479 for the regressions ($100 \times 100 \times 8 \times 8 \times 6 \times 3$; see Table 2). Ozone trends are calculated based
480 on the EESC loading or using a piecewise linear trend (PWLT) analysis. For the PWLT
481 ensembles the three different EESC scenarios are irrelevant. Instead, the sensitivity of the
482 regressions is tested using three different break years (1997, 1998 and 1999). In total we
483 analyze approximately 23 million 000 different trends using the EESC and PWLT
484 scenarios.

485 Note that by basing our analysis on both different ozone and EP flux scenarios certain
486 time-lag relations are taken into account. It should also be noted that the use of such a
487 wide range of scenarios indicates that much remains unclear about what best describes
488 Antarctic ozone depletion and the time-lag relations between ozone and explanatory
489 variables.

490

491 **3 Scenario analysis**

492

493 **3.1 Reproducing Kuttippurath et al., [2013].**

494

495 First a multi-variate regression is performed similar to Kuttippurath et al. [2013] in
496 which the MSR dataset is used within the Vortex core (70°-90°S). The results are
497 summarized in their Figure 5 and Table 4 which are duplicated here in Table 3 along with
498 the results from a multi-variate regression based on the same variables as used in
499 Kuttippurath et al. [2013].

500 Our results reproduce the results from Kuttippurath et al. [2013], although there are
501 minor differences in the absolute numbers, most likely related to differences in EP fluxes
502 [Jayanarayanan Kuttippurath, *personal communication*, September 2013]. The trends for
503 the periods 1979-1999 and for 2000-2010 are of comparable magnitude in both studies,
504 as well as the PWLT significance levels for the period 1979-1999 and the EESC trends
505 for both 1979-1999 and 2000-2010. The magnitude of the recovery for 2000-2010 based
506 on the PWLT is slightly larger, but also in our analysis the post 2010 linear trend in
507 ozone is significant beyond 2σ . For the correlation of the regression model with the ozone
508 record we obtain a value of 0.87 (R^2) comparable to the 0.90 (R^2) reported in
509 Kuttippurath et al., [2013]. Thus, the results are sufficiently similar to proceed with
510 studying the effects of the uncertainties in regressors and ozone record scenarios on the
511 regression results. Note that we calculate the pre-break and post-break EESC-based
512 trends by applying linear regressions to the EESC curve multiplied with the EESC
513 regression coefficient for the pre-break and post-break time periods. As a result, EESC-
514 based trend errors are related to the non-linearity of the EESC curve, and the trend errors
515 differ for both the pre-break and post-break time periods. Our EESC-based trend errors
516 differ from those in Kuttippurath et al (2013), which lacks a description of how EESC-
517 based trend errors are calculated.

518

519 **3.2 Ozone record and regressor correlations.**

520

521 Before analyzing the ensemble of regression results it is important to investigate the
522 correlations between the different regressors. If correlations between regressors are too
523 large, they cannot be considered to be independent, and it should be decided which one to
524 omit from the analysis, as the regression otherwise cannot separate which variability is
525 related to which regressor. Furthermore, it is *a priori* useful to understand how regressors
526 correlate with the ozone record, as a small correlation implies that a regressor can only
527 explain a limited amount of ozone variability.

528 Table 4 shows the mean correlation between the different regressors and their 2σ spread
529 based on the ozone record and regressor selections and/or Monte Carlo results (SAM,
530 SF×QBO index). The EP flux correlates positively with the EESC and negatively with
531 the SAM and, to a lesser extent, also with the SF×QBO index. The other regressors do
532 not show significant cross-correlations. Only for a few individual ozone record scenarios,
533 regressor selections and Monte Carlo results cross-correlations are found to exceed 0.5.

534 The uncertainty in the correlations with the ozone records ranges between about 10%
535 and 20% for each of the regressors. Small cross-correlations between the regressors
536 however do not provide a justification for *a priori* omitting one of the regressors.

537

538 **3.3 Trends.**

539

540 Figure 4 shows the probability distributions of the ozone trends for 1979- Y_B and Y_B -
541 2012 periods, in which Y_B is the break year which can either be 1997, 1998 or 1999. For
542 the 1979- Y_B period the mean EESC trend is -5.56 DU/year (-4.00 to -7.06; 95% CI) and
543 the mean PWLT trend is -6.40 DU/year (-4.22 to -7.18; 95% CI). For the Y_B -2012 period
544 the mean EESC trend is +1.97 DU/year (+0.84 to +3.32 DU/year; 95% CI), and the mean
545 PWLT trend is +3.18 DU/year (+1.66 to +4.74; 95% CI).

546 For the 1979- Y_B period the distributions of EESC and PWLT trends (top panel) are
547 rather similar, although the PWLT correlations show a larger peak towards high
548 correlations compared to the EESC correlations (bottom panel). However, for the Y_B -
549 2012 trends the probability distributions are very different (middle panel). The EESC
550 trends show a tri-modal distribution, because only three different EESC curves were
551 used. These three EESC curves differ predominantly in their post-1997 EESC trends (see
552 also Figure 3). In addition, the tri-modal EESC trend probability distribution for Y_B -2012
553 (middle panel) shows that in the linear regression the EESC fit is determined by the 1979-
554 Y_B period more than by the Y_B -2012 period, as the pre-break trend distribution does not
555 show the same tri-modal shape. This is not surprising because the trends for the 1979- Y_B
556 period are larger and cover a longer period than for Y_B -2012.

557 The correlations distributions (lower panel) are similar for the lowest and highest
558 correlations for both the EESC and PWLT regressions, but in the bulk of the distribution
559 the PWLT results in systematically higher correlations than the EESC regressions.

560 The upper two panels of Figure 4 also include the 1979-1999 and 2000-2012 PWLT
561 trends and 2σ errors as reported in Table 2. The uncertainty range of the 2000-2012
562 PWLT trend in Table 2 and the range in Figure 4 are quite similar. However, the

563 uncertainty range of the 1979-1999 PWLT trend in Table 2 is considerably smaller. This
564 shows that uncertainties in the 1979-1999 ozone trends are larger than estimated by a
565 single regression estimated even though all 1979-1999 trends are statistically significant.

566 The auto-correlation of the ozone residuals is small (one-year lag values are
567 approximately zero), indicating that the auto-correlation present in the ozone record (*e.g.*
568 Fioletov and Shepherd, 2003; Vyushin et al., 2007) is related to some of the processes
569 described by the regression parameters and are removed by the multi-variate regression.
570 Auto-correlation thus does not have to be taken into account in the trend significance
571 calculation.

572

573 **3.4 Regression model performance: sensitivity to the independent variables**

574

575 Sensitivities of the PWLT-based and EESC-based regressions to the ozone and EP flux
576 scenarios are shown in Figure 5. PWLT-based regressions show that the PWLT
577 distribution peak at high correlations is a consistent feature of different ozone records
578 (*Sep-Nov, Sep-Oct, Sep, 7 Sep - 13 Oct, worst 30 days*). Similarly, use of several different
579 EP fluxes also aligns with the PWLT correlation distribution peak, in particular the EP
580 flux scenarios that include both the August and September months. For ozone,
581 correlations get smaller for, respectively, the longest period (19 July – 1 December),
582 shortest period (21-30 September) and October averages.

583 Figure 6 shows the probability distribution of volcanic aerosols for both the PWLT and
584 EESC regressions. Volcanic aerosols have little impact on the explanatory power of the
585 regression results, as already indicated by lack of correlation of this regressor with the

586 ozone record. The PWLT regression coefficient values show that the effect of volcanic
587 aerosols on ozone can be either positive or negative, largely depending on the assumed
588 amount of Pinatubo aerosols relative to El Chichón aerosols, although the distribution
589 predominantly suggests positive regression values. The EESC regressions show a similar
590 sign dependence of ozone on volcanic aerosol, but with no clear sign of the regression
591 value. None of other parameters (EPFLUX scenario, Ozone scenario) have a sign-
592 dependent effect on the aerosol regression coefficient value for both the EESC and
593 PWLT scenarios. The strong sensitivity of the volcanic aerosol regression value –
594 including sign changes – to either aerosol or EESC scenario indicates that including
595 volcanic aerosols is not very important for the multivariate regression and better should
596 be excluded altogether from multi-variate regressions due to insufficient information in
597 the Antarctic ozone record to constrain the ozone – volcanic aerosol relation.

598 For the solar flux – QBO index (Figure 7, panel A) we find no clear dependence of
599 regression coefficient values on any of the scenarios or parameters. The probability
600 distributions for both the EESC and PWLT regressions are very similar. Hence, like for
601 volcanic aerosols, the solar-QBO parameter better should be excluded altogether from
602 multi-variate regressions because the Antarctic ozone record also contains insufficient
603 information to constrain the ozone – solar-QBO relation

604 The SAM regression coefficient values show a continuous random distribution while
605 the overall dependence is predominantly negative (Figure 7, panel B). A positive phase of
606 the SAM correlates with more ozone depletion than a negative phase of the SAM. This is
607 a well-known two-way effect: tropospheric circulation changes affect Antarctic
608 stratospheric ozone on the short term, while the long term changes in Antarctic ozone

609 have affected the tropospheric circulation in the Southern Hemisphere [Kirtman et al.,
610 2013; IPCC AR5, Ch. 11, section 11.3.2.4.2 and references therein].

611 For the EPFLUX the regressions show a positive dependence (Figure 7. panel C) and a
612 similar distribution for both the EESC and PWLT regression.

613

614 **3.5 Optimal regressor and ozone record scenarios**

615

616 Based on the analysis of the entire ensemble presented here it might be possible to
617 choose an optimal set of regressors as well as an optimal ozone record scenario for
618 Antarctic ozone trend analysis. Volcanic aerosols (Figure 6), the QBO and the solar cycle
619 (Figure 7) are shown to have little effect on the regression and thus better should be
620 excluded. For the EP flux, it appears that including the months August and September
621 leads to a better fit (higher correlations; Tables 4 and 5, Figure 5). For ozone, results
622 suggest that there is no clear optimal time-window over which to calculate average
623 ozone, but it appears that the period should not be too short, not be too long, and should
624 include September and preferably the first half of October (Tables 4 and 5).

625 In addition, the use of three different EESC scenarios results in tri-modal distribution
626 features in several parameters (Figures 3 and 6), suggesting that care has to be taken with
627 in particular the ozone trend values attributed to changes in EESC's. Furthermore, the
628 post-break trends are particularly sensitive to the choice in EESC scenario (Figure 3). It
629 could therefore be argued that using a PWLT for post-break trend estimates is preferred
630 over using the EESC-based post-break trend as its distribution better reflects structural

631 uncertainties in the regression and takes the regression residuals into account for
632 calculation of trend uncertainties.

633 Figure 8 illustrates what the best single regressions in the entire ensemble for all three
634 regression models separately look like. The best EESC-regression correlation ($R^2 = 0.95$)
635 was found for a case with Sep -Nov ozone, Jul-Aug EP flux and an EESC with an age-of-
636 air of 4 years. For the best PWLT-regression correlation ($R^2 = 0.96$) these were the same
637 with 1997 as optimal break year. Reason for the high explanatory power is that in all
638 three cases the SAM anomalies align with strong ozone peaks whereas the solar flux –
639 QBO index variations coincidentally align with the smaller ozone anomalies.

640

641 **4. Discussion: Second stage of ozone recovery and trend significance.**

642

643 Given the broad range of outcomes for the different types of regressions and regressors,
644 an important question is not only if ozone has started to increase after the late 1990s, but
645 also whether the trend is statistically significant and can be attributed to declining
646 stratospheric halogens, which is required by WMO for the second stage of ozone
647 recovery to be formally identified. Because the EESC curve-shape is prescribed, there is
648 no degree of freedom allowing for different pre-break and post-break trends in the EESC
649 regression. As discussed in section 2, it is not clear *a priori* which EESC scenario is the
650 optimal choice or if it is even appropriate to use just a single EESC scenario. Hence, how
651 to assign overall uncertainty to the EESC curve remains an open question. Therefore, a
652 better approach would be to investigate whether the PWLT post-break trends are

653 statistically significant as they use the ozone fit residuals for their significance
654 calculation.

655 Figure 9 shows the probability distribution of correlations (R^2) of the PWLT regression
656 models vs. ozone for the entire Monte Carlo dataset, as well as the fraction of post-break
657 PWLT trend estimates that are statistically significant (2σ) for both the periods ending in
658 2010 and 2012. This figure is comparable to Figure 4 (lower panel) and Figure 5, but
659 with larger correlation bins for visualization purposes. Results indicate that trends only
660 become statistically significant beyond a certain explanatory power of the regression
661 model. This is not surprising: only when ozone residuals after removing the regression
662 results are sufficiently small can the post-break trend become statistically significant.
663 This automatically requires a high correlation between the ozone record and the selected
664 regression model. The analysis here shows that statistically significant trends require a
665 correlation (R^2) of at least approximately 0.60. Furthermore, only for high ozone-
666 regression model correlations ($R^2 > 0.80$) the majority of trends become statistically
667 significant.

668 In section 3.5 the results of the ensemble were analyzed to determine optimal scenarios
669 in terms of explanatory power (R^2). However, the second stage of ozone recovery
670 requires also a statistically significant post-break year trend. We therefore analyzed the
671 percentage of statistically significant post-break trends in the ensemble for the PWLT-
672 based regressions. We focus on the ozone record and EP flux scenarios as the
673 uncertainties associated with these two parameters are the most important ones, as
674 discussed before. Table 5 shows the percentage of regressions for each combination of
675 ozone record and EP flux scenarios that is statistically significant for the ozone records

676 ending in 2010. There are large differences in the fraction of statistically significant
677 PWLT-based trends, ranging from less than 0.1% (*21-30 September* average ozone) to a
678 complete 100% significance (*September-October* and *October* ozone, *45S-75S Aug-Sep*
679 *EP flux*). Table 6 shows the same results as Table 5, but only for the break year 1997 and
680 the period ending in 2012. In this case there is a large number of ozone record - EP flux
681 scenario combinations with statistically significant trends. If we would consider only the
682 EP fluxes that include the August and September months, then with the exception of the
683 *21-30 September* time window nearly all trends are statistically significant.

684 Table 7 shows that the number of significant trends further depends on the choice of
685 break year, with the number of statistically significant trends increasing steadily with
686 increasing length of the period over which trends are calculated. This is not surprising as
687 the regression trend error decreases with increasing number of points for which the trends
688 are calculated (Supplementary Information equation S2).

689 Excluding the year 2002 from the regressions has a significant impact on the post-break
690 ozone trends themselves. However, it hardly has any effect on the post-break trends from
691 the regressions (not shown), indicating effective removal of the anomalous year 2002
692 from the results. Excluding volcanic years from the regression had no significant effect
693 on both the ozone trends before and after the regression, consistent with our finding that
694 there appears to be little (direct) impact of volcanic aerosols on Antarctic springtime
695 ozone.

696 It is tempting to interpret, based on some selections of our results, that the significance
697 is sufficient for identification of the second stage of ozone recovery by 2012. However,
698 comparing Table 5 and Table 6 – thus 2000-2010 trends vs 1998-2012 trends – shows

699 that the longer period not always results in increased statistical significance. In particular,
700 the need to average ozone over longer periods of time may introduce long term changes
701 in average ozone that are not related to photochemical ozone destruction. Furthermore,
702 the trend significance is generally between 2σ and 3σ (not shown), indicating that a
703 considerable amount of variability is not accounted for in the regression. In addition, our
704 analysis shows that detection of the 2nd stage of ozone recovery based on just one
705 arbitrary selected (set of) regressor – ozone record combination(s) does not reflect the
706 structural uncertainties present in the underlying data.

707 Nevertheless, the appearance of large groups of statistically significant results occurring
708 for longer time series and a certain persistence among ozone scenarios and EP flux
709 scenarios, shows that these type of analyses are capable of removing deterministic
710 variations in average ozone, and that with increasing length of the post-break period more
711 statistically significant results can be expected.

712

713 **5. Conclusions**

714

715 The primary goal of this study was to investigate whether or not the 2nd stage of ozone
716 recovery – a statistical increase in ozone attributable to ozone depleting substances – can
717 be detected, given uncertainties in underlying data. A detailed sensitivity analysis of
718 widely used multi-variate regression analysis of total ozone columns was presented
719 focusing on Antarctic springtime ozone. By combining regressor scenarios and Monte
720 Carlo simulations for various ozone record scenarios, a total of approximately 23 million
721 different multivariate regressions were performed.

722 Use of the post-break trends based on fitting the EESC to the total ozone record is not
723 recommended, as these trends are solely based on the pre-defined EESC shape and do not
724 allow flexibility in the trend calculation. Because the resulting EESC-fit based trend
725 uncertainties do not take the ozone fit residuals into account the EESC scenarios result in
726 overconfident ozone trend uncertainties, neglecting structural uncertainties and sensitivity
727 to the chosen scenario.

728 Our analysis shows that the EP flux and the SAM effects are capable to explain
729 significant parts of Antarctic ozone variations and the removal of these effects improves
730 the analysis of recovery,, in contrast to the inclusion in the regressions of volcanic
731 aerosols and the combined QBO/Solar flux index.

732 Consistent with expectations, we find a robust gradual small increase in Antarctic
733 ozone since the late 1990s that can be attributed to decreases in ODS for selected
734 combinations of regressors, although the magnitude of the increase is rather uncertain
735 (+1.66 – +4.74 DU/year; 95% CI).

736 The limited information present in the Antarctic ozone record for volcanic aerosols
737 (essentially two isolated peaks) is consistent with Knibbe et al. [2014], who found little
738 evidence for volcanic effects on total ozone throughout the Southern Hemisphere.
739 Furthermore, Poberaj et al. [2011] also reported little impact of volcanic aerosols from
740 the Pinatubo eruption on Southern Hemispheric ozone, attributing it to dynamical
741 conditions favoring more poleward transport of ozone from the tropics and mid-latitudes
742 than usual, thereby “*overcompensating the chemical ozone loss ...and reduce the overall*
743 *strength of the volcanic ozone signal*”.

744 The lack of correlation between Antarctic ozone and the solar-flux/QBO combined
745 index was also found by Knibbe et al. [2014] for both Antarctic (and Arctic) ozone
746 trends. This lack of QBO-solar signal in Antarctic springtime ozone – also e.g. reported
747 in both Labitzke [2004] and Roscoe and Haigh [2007] - may be related to the dominance
748 in absolute values of the ozone change of ozone depletion and vortex dynamics over
749 potential indirect solar influences on Antarctic springtime ozone.

750 From our analysis it remains unclear what the appropriate time window would be over
751 which to average the ozone record and the EP flux. Results indicate that the best
752 regression occur for ozone averaged over a time window that includes the ozone hole
753 season – typically September and part of October. On the other hand, the time window
754 should also not extend far beyond the ozone hole season as more and more non-
755 photochemical ozone variations are introduced in the averaged ozone with a longer
756 averaging period. Similarly, for the EP flux we find that including both the August and
757 September months result in the best regressions. However, the choice for using complete
758 calendar months is rather arbitrary, and better choices may exist which is here left for
759 future research.

760 The lack of a proper definition of appropriate time windows drives our recommendation
761 that care has to be taken with drawing firm conclusions about Antarctic ozone recovery
762 based on multi-variate regression of Antarctic vortex average ozone. It is tempting to
763 discard those results in the full ensemble that do not confirm our expectations, but
764 without proper justification of what constitutes the best set of independent explanatory
765 variables – for example physically compelling arguments - there is the danger of working
766 towards an expected answer.

767 Another last finding is that a longer post-break period does not necessarily always
768 results in more significant trends, which provides yet another indication to remain careful
769 with drawing too firm conclusions from multivariate regressions. On the other hand, it
770 can be expected that with extending the ozone record and using a multi-variate regression
771 method to remove well-selected non-ODS influences from the total ozone record – the
772 second stage of recovery of the Antarctic ozone-hole will be detectable before 2020.
773 Future updates of the analysis in this paper by extension of the present-day ozone records
774 will rather soon provide indications whether this moment approaches fast or not.
775

776 **Acknowledgements**

777 The authors wish to thank the following authors of chapter 3 of the 2014 WMO ozone
778 assessment report – Sophie Godin Beekmann, Martin Dameris, Peter Braesicke, Martin
779 Chipperfield, Markus Rex and Michelle Santee – as well as John Pyle, Ted Shepherd and
780 in particular Paul Newman for encouraging us to write this paper.

781

782 **References**

783

784 Van der A et al. (2010), Multi sensor reanalysis of total ozone *Atm. Chem. Phys.*, 10,
785 11277-11294, doi:10.5194/acp-10-11277-2010.

786 Ammann et al. (2003), A monthly and latitudinally varying volcanic forcing dataset in
787 simulations of 20th century climate, *Geophys. Res. Lett.*, 30, 1657,
788 doi:10.1029/2003GL016875.

789 Andrews et al. (1987), *Middle Atmosphere Dynamics*, Academic Press, Orlando, Florida,
790 489 pp.

791 Anet et al. (2013), Impact of a potential 21st century “grand solar minimum” on surface
792 temperatures and stratospheric ozone, *Geophys. Res. Lett.*, 40, 4420–4425,
793 doi:10.1002/grl.50806.

794 Bekki et al., (2011), *Future Ozone and its impact on surface UV*, Chapter 3 *Scientific*
795 *Assessment of Ozone Depletion: 2010*, Global Ozone Research and Monitoring
796 *Project - Report No. 52*, 516 pp., Geneva, Switzerland.

797 Bunzel and Schmidt (2013), *The Brewer–Dobson Circulation in a Changing Climate:*
798 *Impact of the Model Configuration.* *J. Atmos. Sci.*, 70, 1437–1455. doi:
799 <http://dx.doi.org/10.1175/JAS-D-12-0215.1>

800 Crowley and Unterman (2012), Technical details concerning development of a 1200-yr
801 proxy index for global volcanism, *Earth Syst. Sci. Data Discuss.*, 5, 1-28,
802 doi:10.5194/essdd-5-1-2012.

803 Dameris, M., S. Matthes, R. Deckert, V. Grewe, and M. Ponater (2006), Solar cycle
804 effect delays onset of ozone recovery, *Geophys. Res. Lett.*, 33, L03806,
805 doi:[10.1029/2005GL024741](https://doi.org/10.1029/2005GL024741).

806 De Laat and van Weele, (2011) The 2010 Antarctic ozone hole: Observed reduction in
807 ozone destruction by minor sudden stratospheric warmings, *Sci. Rep.*, 1, 38, doi:
808 10.1038/srep00038.

809 Dudok de Wit et al. (2009), Finding the best proxies for the solar UV irradiance,
810 *Geophys. Res. Lett.*, 36, L10107, doi:10.1029/2009GL037825.

811 Ebdon (1960): Notes on the wind flow at 50 mb in tropical and sub-tropical regions in
812 January 1957 and January 1958. *Q. J. Roy. Met. Soc.*, 86, 540-542.

813 Engel et al. (2009), Age of stratospheric air unchanged within uncertainties over the past
814 30 years, *Nature Geoscience* 2, 28 – 31, doi:10.1038/ngeo388.

815 Eyring, et al. (2007), Multimodel projections of stratospheric ozone in the 21st century, *J.*
816 *Geophys. Res.*, 112, D16303, doi:10.1029/2006JD008332.

817 Fioletov, V. E., and T. G. Shepherd (2003), Seasonal persistence of midlatitude total
818 ozone anomalies, *Geophys. Res. Lett.*, 30, 1417, doi:[10.1029/2002GL016739](https://doi.org/10.1029/2002GL016739).

819 Graystone (1959), Meteorological office discussion on tropical meteorology. *Met.*
820 *Magazine*, 88, 117.

821 Haigh, J.D., The impact of solar variability on climate (1996), *Science*, Vol. 272, no.
822 5264 pp. 981-984, DOI: 10.1126/science.272.5264.981

823 Haigh and Roscoe (2006), Solar influences on polar modes of variability,
824 *Meteorologische Zeitschrift*, Volk.15, pp. 371-378

825 Ho et al. (2012) The Southern Annular Mode: a comparison of indices, *Hydrol. Earth*
826 *Syst. Sci.*, 16, 967-982, doi:10.5194/hess-16-967-2012.

827

828 Hood, L. (1997), The solar cycle variation of total ozone: Dynamical forcing on the lower
829 stratosphere, *Journal of Geophysical Research*, 102(D1), 1355-1370.

830 Huang and Massie (1997), Effect of volcanic particles on the O₂ and O₃ photolysis rates
831 and their impact on ozone in the tropical stratosphere, *J. Geophys. Res.*, 102(D1),
832 1239–1249, doi:10.1029/96JD02967.

833 Jiang et al. (2008): Interannual Variability and Trends of Extratropical Ozone. Part II:
834 Southern Hemisphere. *J. Atmos. Sci.*, 65, 3030–3041, doi: 10.1175/2008JAS2793.1

835 Kalnay, E., et al. (1996). The NCEP/NCAR 40-Year Reanalysis Project, *Bull. Am. Met.*
836 *Soc.*, **77** (3): 437–471.

837 Kirtman et al. (2013), Near-term Climate Change: Projections and Predictability. In:
838 Climate Change 2013: The Physical Science Basis. Contribution of Working Group I
839 to the Fifth Assessment Report of the Intergovernmental Panel on Climate Change,
840 Stocker et al. (EDS.), Cambridge University Press, Cambridge, United Kingdom and
841 New York, NY, USA, *in press*.

842 Klekociuk et al. (2011), The Antarctic ozone during 2010, *Australian Meteorological and*
843 *Oceanographic Journal*, 61 (4), 253-267.

844 Knibbe, J. S., et al. (2014), Spatial regression analysis on 32 years of total column ozone
845 data, *Atmos. Chem. Phys.*, 14, 8461-8482, doi:10.5194/acp-14-8461-2014,.

846 Kramarova et al. (2014), Measuring the Antarctic ozone hole with the new Ozone
847 Mapping and Profiler Suite (OMPS), *Atmos. Chem. Phys.*, 14, 2353-2361,
848 doi:10.5194/acp-14-2353-2014.

849 Kuttippurath et al. (2010), Estimation of Antarctic ozone loss from ground-based total
850 column measurements, *Atmos. Chem. Phys.*, 10, doi: 10.5194/acp-10-6569-2010,
851 6569-6581.

852 Kuttippurath et al., Antarctic ozone loss in 1979–2010 (2013) first sign of ozone
853 recovery, *Atmos. Chem. Phys.*, 13, doi: 10.5194/acp-13-1625-2013, 1625-1635,.

854 Labitzke (2004), On the signal of the 11-Year sunspot cycle in the Stratosphere over the
855 Antarctic and its modulation by the Quasi-Biennial Oscillation (QBO),
856 *Meteorologische Zeitschrift*, Vol. 13, No. 4, 263-270.

857 McCormack, J. P., & Hood, L. L. (1996). Apparent solar cycle variations of upper
858 stratospheric ozone and temperature: Latitude and seasonal dependences. *Journal of*
859 *Geophysical Research: Atmospheres*, 101(D15), 20933-20944.

860 Naujokat (1986), An update of the observed quasi-biennial oscillation of the stratospheric
861 winds over the tropics. *J. Atmos. Sci.*, 43, 1873-1877.

862 Newman et al. (2006), When will the Antarctic ozone hole recover? *Geophys. Res. Lett.*,
863 33, L12814, doi:10.1029/2005GL025232.

864 Newman et al. (2007), A new formulation of equivalent effective stratospheric chlorine
865 (EESC), *Atmos. Chem. Phys.*, 7, 4537-4552, doi:10.5194/acp-7-4537-2007.

866 Poberaj et al. (2011): Missing Stratospheric Ozone Decrease at Southern Hemisphere
867 Middle Latitudes after Mt. Pinatubo: A Dynamical Perspective. *J. Atmos. Sci.*, 68,
868 1922–1945. doi: <http://dx.doi.org/10.1175/JAS-D-10-05004.1>

869 Randel et al. (2002), Changes in column ozone correlated with the stratospheric EP flux,
870 J. Meteor. Soc. Jap., 80, 4b, 849-862.
871

872 Rozanov et al. (2002), Climate/chemistry effects of the Pinatubo volcanic eruption
873 simulated by the UIUC stratosphere/troposphere GCM with interactive
874 photochemistry, J. Geophys. Res., 107(D21), 4594, doi:10.1029/2001JD000974.

875 Salby et al. (2011), Rebound of Antarctic ozone, *Geophys. Res. Lett.*, 38, L09702, doi:
876 10.1029/2011GL047266.

877 Salby et al. (2012), Changes of the Antarctic ozone hole: Controlling mechanisms,
878 seasonal predictability, and evolution, *J. Geophys. Res.*, 117, D10111, doi:
879 10.1029/2011JD016285.

880 Sato et al. (1993), Stratospheric aerosol optical depths, 1850-1990. *J. Geophys. Res.*, 98,
881 22987-22994, doi:10.1029/93JD02553.

882 Solomon, S., et al. (2011), The persistently variable “background” stratospheric aerosol
883 layer and global climate change. *Science*, Vol. 333, no. 6044, pp. 866-870, doi:
884 10.1126/science.1206027

885 Soukharev and Hood (2006), Solar cycle variation of stratospheric ozone: Multiple
886 regression analysis of long-term satellite data sets and comparisons with models, *J.*
887 *Geophys. Res.*, 111, D20314, doi:10.1029/2006JD007107.

888 Stiller et al. (2008), Global distribution of mean age of stratospheric air from MIPAS SF6
889 measurements, *Atmos. Chem. Phys.*, 8, 677-695, doi:10.5194/acp-8-677-2008.

890 Telford et al. (2009), Reassessment of causes of ozone column variability following the
891 eruption of Mount Pinatubo using a nudged CCM, *Atmos. Chem. Phys.*, 9, 4251-
892 4260, doi:10.5194/acp-9-4251-2009, 2009.

893 Thompson, D.W.J. and J.M. Wallace (2000): Annular Modes in the Extratropical
894 Circulation, Part I: Month-to-Month Variability, *J. Climate*, 13, 1000–1016.

895

896 United Nations Environment Programme (2012), *The Montreal Protocol on Substances*
897 *that Deplete the Ozone Layer*, Nairobi, Kenya, ISBN 978-9966-20-009-9.

898 Vernier, J.-P., et al. (2011), Major influence of tropical volcanic eruptions on the
899 stratospheric aerosol layer during the last decade, *Geophys. Res. Lett.*, 38, L12807,
900 doi:10.1029/2011GL047563.

901 Vyushin, D., V. E. Fioletov, and T. G. Shepherd (2007), Impact of long-range
902 correlations on trend detection in total ozone, *J. Geophys. Res.*, 112, *D14307*,
903 doi:[10.1029/2006JD008168](https://doi.org/10.1029/2006JD008168)

904 Weber et al. (2003), Dynamical control of NH and SH winter/spring total ozone from
905 GOME observations in 1995-2002, *Geophys. Res. Lett.*, 30, 1853, doi:
906 10.1029/2002GL016799.

907 Weber et al. (2011), The Brewer-Dobson circulation and total ozone from seasonal to
908 decadal time scales, *Atmos. Chem. Phys.*, 11, 11221-11235, doi: 10.5194/acp-11-
909 11221-2011.

910 World Meteorological Organization (2007), *Scientific Assessment of Ozone Depletion:*
911 *2006*, Global Ozone Research and Monitoring Project - Report No. 50, 572 pp.,
912 Geneva, Switzerland.

913 World Meteorological Organization (2011), Scientific Assessment of Ozone Depletion:
914 2010, Global Ozone Research and Monitoring Project - Report No. 52, 516 pp.,
915 Geneva, Switzerland.

916 Yang, E.-S., D. M. Cunnold, M. J. Newchurch, R. J. Salawitch, M. P. McCormick, J. M.
917 Russell III, J. M. Zawodny, and S. J. Oltmans (2008), First stage of Antarctic ozone
918 recovery, *J. Geophys. Res.*, 113, D20308, doi:[10.1029/2007JD009675](https://doi.org/10.1029/2007JD009675).

919

920Tables

<p>EP flux</p> <p>http://www.awi.de/en/research/research_divisions/climate_science/atmospheric_circulations_old/projects/candidoz/ep_flux_data/</p>
<p>QBO</p> <p>http://www.geo.fu-berlin.de/met/ag/strat/produkte/qbo/</p>
<p>Solar flux</p> <p>ftp://ftp.geolab.nrcan.gc.ca/data/solar_flux/monthly_averages/solflux_monthly_average.txt</p>
<p>SAM</p> <p>ftp://ftp.cpc.ncep.noaa.gov/cwlinks/</p>
<p>EESC</p> <p>http://acdb-ext.gsfc.nasa.gov/Data_services/automailer/</p>
<p>Volcanic aerosol</p> <p>http://data.giss.nasa.gov/modelforce/strataer/</p>
<p>Assimilated total ozone</p> <p>http://www.temis.nl/protocols/O3global.html</p>

921 **Table 1.** Data sources

922

regressor	variations
<p>Average EP flux - 8 scenarios</p>	<ul style="list-style-type: none"> - 70 hPa, 40°S-90°S, Aug-Sep (baseline) - 70 hPa, 40°S-90°S, Jul-Aug - 70 hPa, 40°S-90°S, Jul-Sep - 70 hPa, 40°S-90°S, Jul - 70 hPa, 40°S-90°S, Aug - 70 hPa, 40°S-90°S, Sep - 70 hPa, 45°S-75°S, Aug-Sep - 100 hPa, 40°S-90°S, Aug-Sep
<p>Solar flux – QBO index - 100 Monte Carlo series</p>	<ul style="list-style-type: none"> - Random variations in Solar flux – QBO anomalies - 200% Gaussian noise variations on single solar flux – QBO anomalies

SAM index - 100 Monte Carlo series	- 100% random error on annual mean SAM index values
EESC loading - 3 scenarios	- EESC shapes based on different age of air of 2.5, 4.0 and 5.5 years
Volcanic aerosol - 6 scenarios	<ul style="list-style-type: none"> - Baseline Volcanic Aerosol index (NASA GISS) - Pinatubo peak scaled to El Chichón peak - Pinatubo peak 2.5 times the El Chichón peak - Pinatubo peak 5 times the El Chichón peak - El Chichón peak shifted one year back compared to Pinatubo peak - Pinatubo peak shifted one year back compared to El Chichón peak
Ozone record - 8 scenarios	<ul style="list-style-type: none"> - Sep-Oct-Nov average ozone (baseline) - Sep-Oct average ozone - Sep average ozone - Oct average ozone - 7 Sep – 13 Oct average ozone - Very short 21-30 Sep average ozone - Very long 19 Jul – 1 Dec average ozone - “Worst” 30-day average ozone.

923 **Table 2.** Summary of the uncertainties for the proxies discussed in section 2.1 to 2.9 and

924 their inclusion in the regression analysis in this study.

925

Period	Kuttippurath et al. [2013]		This study	
	EESC	PWLT	EESC	PWLT
1979-1999	-4.50 ± 0.65	-5.02 ± 1.11	-5.39 ± 0.22	-5.66 ± 1.03
2000-2010	1.11 ± 0.16	2.91 ± 2.73	1.04 ± 0.12	3.30 ± 2.85
1979-1999			-5.26 ± 0.21	-5.75 ± 1.00
2000-2012			1.09 ± 0.10	3.28 ± 2.49

927 **Table 3.** EESC-based Antarctic vortex core ozone trends and their 2σ trend uncertainties
928 (DU/year) derived from multi-variate linear regression. The trends in ozone based on EESC
929 regression are calculated by an Ordinary Linear Regression based of the pre-defined
930 change in EESC multiplied with the EESC regression coefficient for the time period
931 under consideration [*cf.* Kuttippurath et al., 2013]. The EESC trend is in pptv/year, the
932 EESC regression coefficient is in DU/pptv, hence the trend in ozone is in DU/year,
933 allowing direct comparison with the PWLT ozone trends (also in DU/year)

934

	EPFLUX	EESC	AEROSO L	SF×QBO
SAM	-0.31 ± 0.27	-0.03 ± 0.17	-0.09 ± 0.19	-0.09 ± 0.29
SF×QBO	0.08 ± 0.28	0.07 ± 0.42	-0.02 ± 0.19	
AEROS OL	0.05 ± 0.17	0.03 ± 0.30		
EESC	0.25 ± 0.17			

935 **Table 4.** Cross correlations and their 2σ variance between explanatory variables.

936

EP flux \ Ozone								
	Aug - Sep	Jul - Aug	Jul - Sep	Jul	Aug	Sep	45°S-75°S	100 hPa
Sep - Nov	27.7	16.9	43.5	2.3	18.2	2.6	84.9	70.7
Sep - Oct	98.5	80.7	99.7	37.5	71.5	71.2	100.0	100.0
Sep	34.8	23.1	41.9	5.0	23.0	15.0	60.8	60.4
Oct	99.4	72.5	99.2	35.2	63.7	77.6	100.0	99.9
21 - 30 Sep	<0.1	<0.1	<0.1	<0.1	<0.1	<0.1	1.0	1.9
7 Sep – 13 Oct	54.3	19.5	55.2	5.3	17.8	24.4	92.1	90.7
Worst 30 days	87.3	52.9	94.2	18.8	42.2	53.6	99.6	99.1
19 Jul – 1 Dec	30.1	21.8	36.3	4.6	27.4	5.3	78.6	68.2

938 **Table 5.** Percentage of statistically significant regressions for each combination of ozone
 939 and EP flux scenarios, as defined in section 2, based on the PWLT regression model.
 940 Each ensemble consists of results of 180,000 single regressions (6 volcanic aerosol
 941 scenarios, 100 SAM and 100 QBO-solar index Monte Carlo runs, 3 break years).
 942 Numbers in bold are statistically significant > 95%.

943

EP flux \ Ozone								
	Aug - Sep	Jul - Aug	Jul - Sep	Jul	Aug	Sep	45°S-75°S	100 hPa
Sep - Nov	99.9	10.7	92.6	0.1	36.3	29.5	100.0	100.0
Sep - Oct	100.0	52.2	100.0	4.2	73.4	100.0	100.0	100.0
Sep	100.0	40.3	99.5	2.0	67.5	96.4	100.0	100.0
Oct	100.0	12.1	98.0	0.6	27.2	98.1	100.0	100.0
21 - 30 Sep	0.1	<0.1	<0.1	<0.1	<0.1	<0.1	2.0	20.9
7 Sep – 13 Oct	100.0	10.0	97.7	0.8	19.6	98.4	100.0	100.0
Worst 30 days	100.0	20.0	99.4	1.2	29.6	99.7	100.0	100.0
19 Jul – 1 Dec	99.9	25.6	95.3	1.5	66.1	56.5	100.0	100.0

944 **Table 6.** As table 5 but for the break year 1997 and the period ending in 2012.

945

Start year	End year	Length (years)	significant trends
2000	2010	11	34.3%
1999	2010	12	47.8%
1998	2010	13	59.5%
all	2010		47.3%
2000	2012	13	39.0%
1999	2012	14	52.7%
1998	2012	15	60.7%
all	2012		50.5%

946 **Table 7.** Fraction of statistically significant trends (%) in all regression results for
947 different break years, period lengths and different types of trend calculations. The start
948 year and end year refer to the time period for which trends are calculated. The “all” start
949 years refers to the statistics for all three start years scenarios combined.

950

951

952 **Supplementary information**

953

954

955 **QBO.**

956

957 The Quasi-Biennial Oscillation (QBO) of the winds in the equatorial stratosphere has
958 been discovered in the 1950s through the establishment of a global, regularly measuring
959 radiosonde network [Graystone, 1959; Ebdon, 1960]). The Free University of Berlin has
960 compiled a long-term record from 1953 onwards of daily wind observations of selected
961 stations near the equator. From these daily measurements monthly mean zonal
962 components were calculated for pressure levels of 70, 50, 40, 30, 20, 15, and 10 hPa. For
963 the period after 1979 only measurements from Singapore are used. The QBO data set is
964 supposed to be representative of the equatorial belt since various studies have shown that
965 longitudinal differences in the phase of the QBO are small [Hood, 1997]. It should be
966 noted, however, that some uncertainties arose at higher levels during the early years from
967 the scarcity of observations. More information on the original data and their evaluation
968 can be found in Naujokat [1986].

969 As proxy for the regressions we will use the 40-hPa QBO index, also used in
970 Kuttippurath et al. [2013]. Salby et al. [2011, 2012] chose to use 30-hPa winds instead.
971 The relevancy of the choice of QBO index will be evaluated later. Information on the
972 uncertainties in the monthly QBO data is not available. One indirect method to estimate
973 the uncertainties is by examining QBO index variability close to the maximum and
974 minimum of the QBO cycles, where the QBO index values remains more or less constant
975 for some months. Assuming that during the maximum or minimum in the QBO phase
976 variations from month to month are indicative of uncertainties in the QBO, we come up
977 with estimated uncertainties of around 1.5-2.0 m/s in the zonal mean wind speeds.

978

979 **Solar flux**

980

981 Variations in incoming solar radiation – in particular the shorter ultraviolet wavelengths
982 – have an effect on stratospheric ozone [Haigh, 1996; McKormack and Hood, 1996;
983 Soukharev and Hood, 2006; Anet et al., 2013]. A standard proxy for variations in
984 incoming solar radiation in ozone regression studies is to use the monthly mean 10.7 cm
985 radio flux, as also used in Kuttippurath et al. [2013]. This data set was obtained via
986 NOAA/NESDIS/NGDC/STP.

987 However, there are other solar activity proxies available. Ideally, in absence of true UV
988 spectral measurements, one would like to use a proxy that is representative for solar
989 activity at those wavelengths where stratospheric ozone formation occurs, which is of
990 roughly between 200 and 300 nm. Dudok de Wit et al. [2009] tried to identify the best
991 proxy for solar UV irradiance, and concluded that proxies derived from a certain
992 wavelength range best represent the irradiance variations in that wavelength band. Thus,
993 the 10.7-cm radio flux might not fully represent solar UV variability. Using the results
994 from Dudok and de Wit et al. [2009] to analyze a set of seven solar activity proxies
995 dating back to at least 1979 based on the solar2000 model and obtained from
996 NOAA/NESDIS/NGDC/STP (F10.7, Lyman-alpha, E10.7, and the solar constant S), we
997 will assume in our regressions that the uncertainty range associated with the solar proxy
998 is approximately 15% of the root-mean-square of the anomaly values.

999

1000 **Why do standard errors of an ordinary linear regression relative to the regression**
1001 **slope not depend on the actual regression itself?**

1002

1003 This analysis is based on the “Data Analysis Toolkit” document (chapter 10), written by
1004 Prof. James Kircher, Professor of Earth and Planetary Science at the University of
1005 California, Berkley and emeritus Goldman Distinguished Professor for the Physical
1006 Sciences.

1007

1008 <http://seismo.berkeley.edu/~kirchner/>

1009

1010 The standard error of the regression slope **b** of an ordinary linear regression of two
1011 variables **x** and **y**, and the regression slope **b** itself can be written as:

1012

1013
$$s_b = \frac{b}{\sqrt{n-2}} \sqrt{\frac{1}{r^2} - 1} \quad \text{and} \quad b = r \frac{S_y}{S_x} \quad (\text{S1})$$

1014 In which **s_b** is the standard error of the regression slope, **n** the number of data points of
1015 the variables **x** and **y**, **r** is the Pearson correlation coefficient between the variables **x** and
1016 **y**, and **S_{x,y}** is the standard deviation of the variables **x** and **y**.

1017 For a statistically significant trend one generally defines that the trends (slopes) should
1018 exceed two times the standard error. Or, in other words, the standard error of the
1019 regression slope divided by the regression slope itself should be less than 0.5

1020 The standard error of the regression slope relative to the regression slope itself – which
1021 directly relates to statistical significance of the trend - becomes, based on the equation
1022 above:

1023

$$s_b / b = \frac{1}{\sqrt{n-2}} \sqrt{\frac{1}{r^2} - 1} \quad (\text{S2})$$

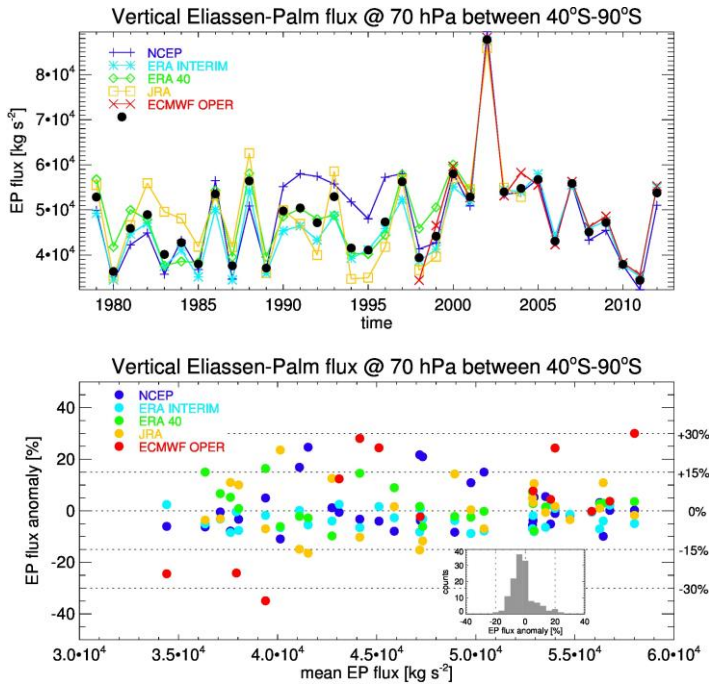
1024 which only depends on the correlation between the variables **x** and **y** and the number of

1025 data points of variable **x** and **y** (record length).

1026

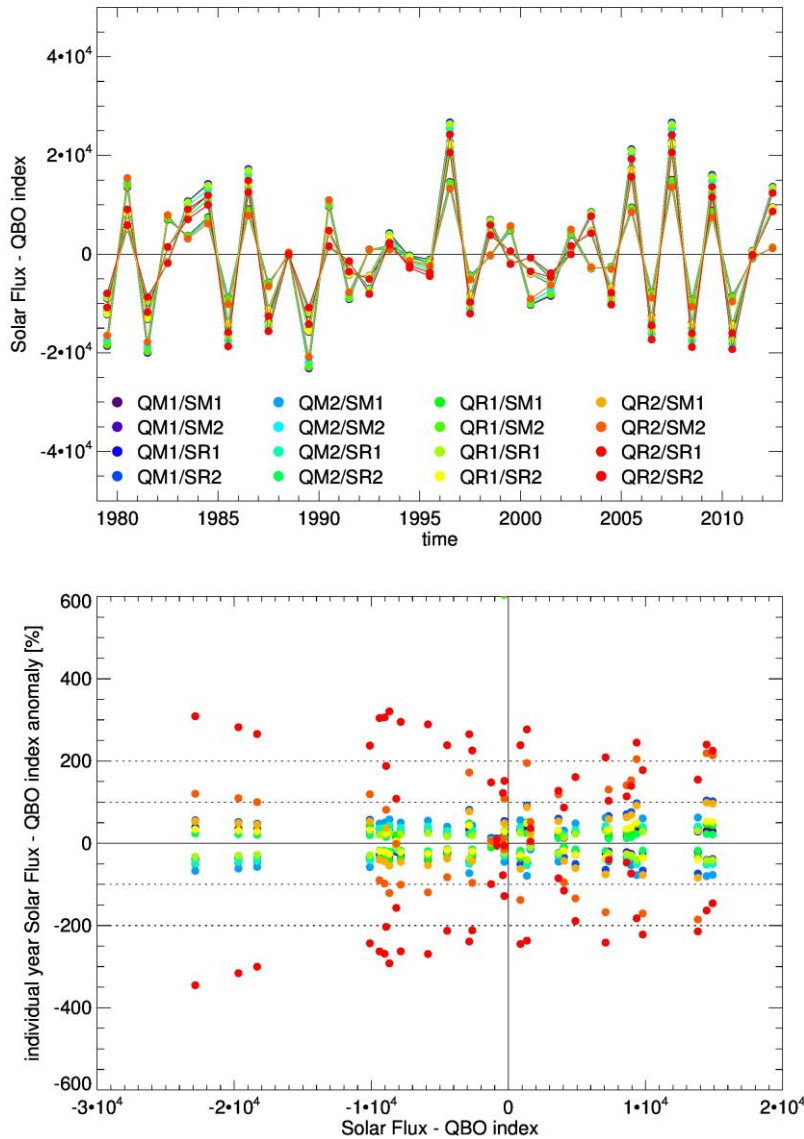
1 **Figures**

2



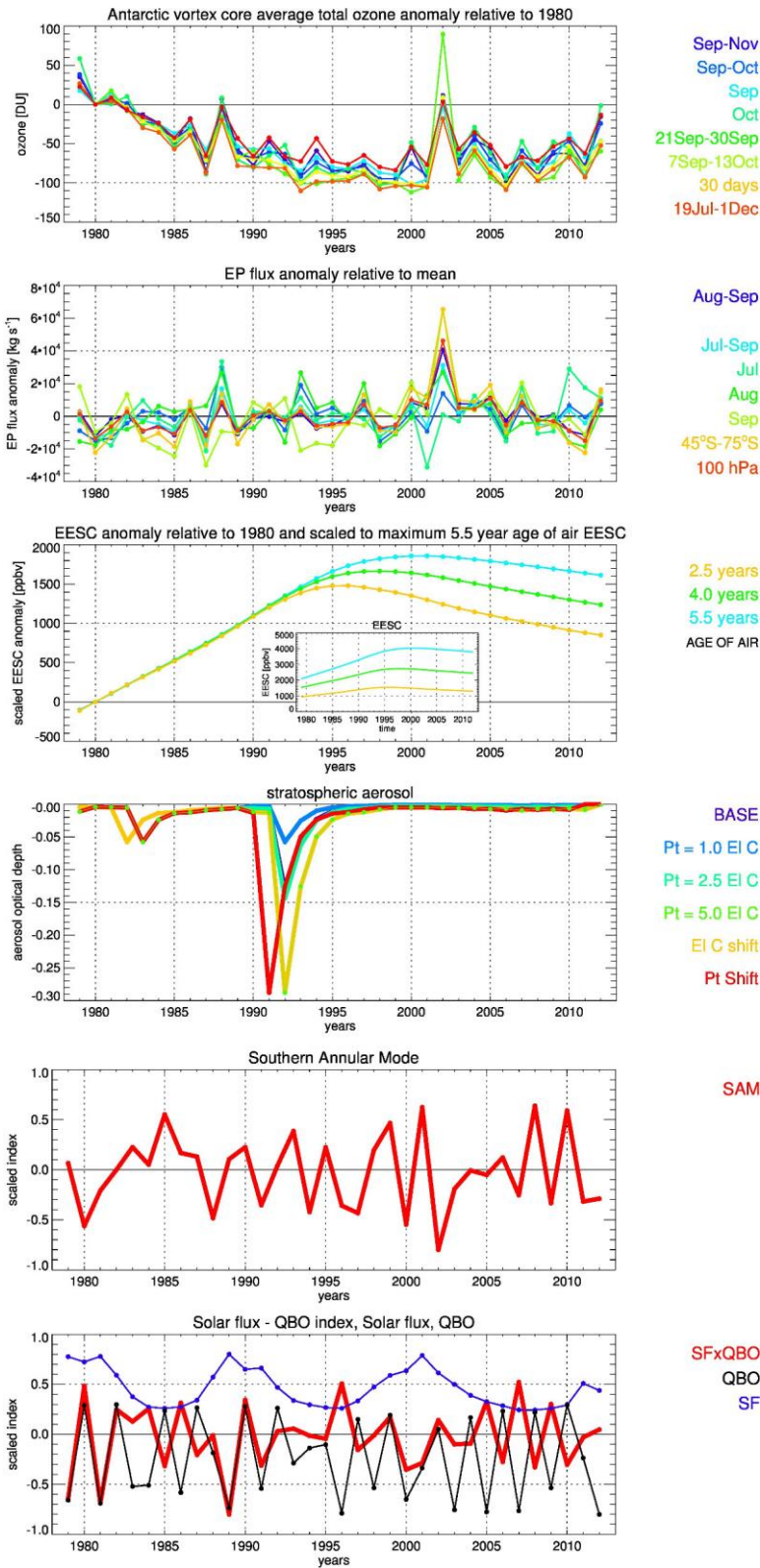
3

4 **Figure 1.** Vertical Eliassen-Palm (EP; kg/s^2) flux at 70 hPa between 40°S and 90°S for
5 five different meteorological datasets for the period 1979-2012 averaged for the two
6 month period August-September: NCEP reanalysis 1979-2012, ECMWF ERA INTERIM
7 1979-2012, ECMWF ERA 40 1979-2001, Japan Reanalysis 1979-2005, ECMWF
8 operational analysis 1998-2012. Top panel shows the EP flux as function of time,
9 including the mean EP flux for each year based on all datasets. Bottom panel shows the
10 EP flux anomalies (%) of a given year as function of the mean EP flux (black dots in the
11 upper panel) for all meteorological datasets available for that year. The insert shows the
12 probability distribution of the relative anomalies. Data are obtained from the EP flux data
13 website of the Alfred Wegener Institute (AWI) for Polar and Marine Research in
14 Bremerhaven, Germany.

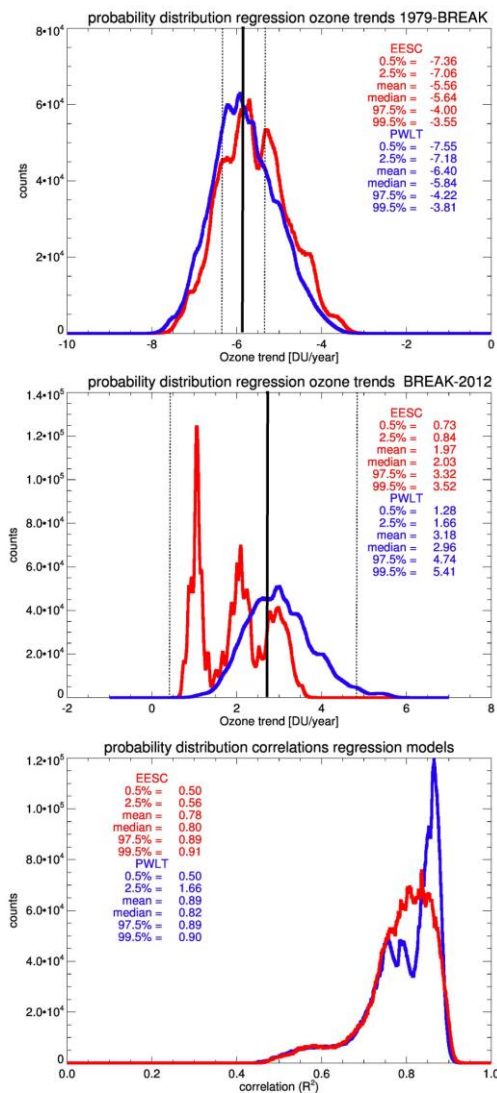


15

16 **Figure 2.** Time series of the combined Solar flux- QBO index (arbitrary units) (upper
 17 plot) and the index anomalies relative to the average of different possibilities to derive at
 18 the index. The Solar flux (“S”) and QBO (“Q”) anomalies were calculated based both on
 19 the average (“M”) as well as the range of Solar flux and QBO values (“R”, see section 2.5
 20 for the explanations of the “range”), and for both the entire record of Solar flux and QBO
 21 values (1947-2012 and 1953-2012, respectively; “1”) as well as for the period 1979-2012
 22 (“2”), resulting in a total of 16 combinations. The different colors denote the different
 23 combinations.

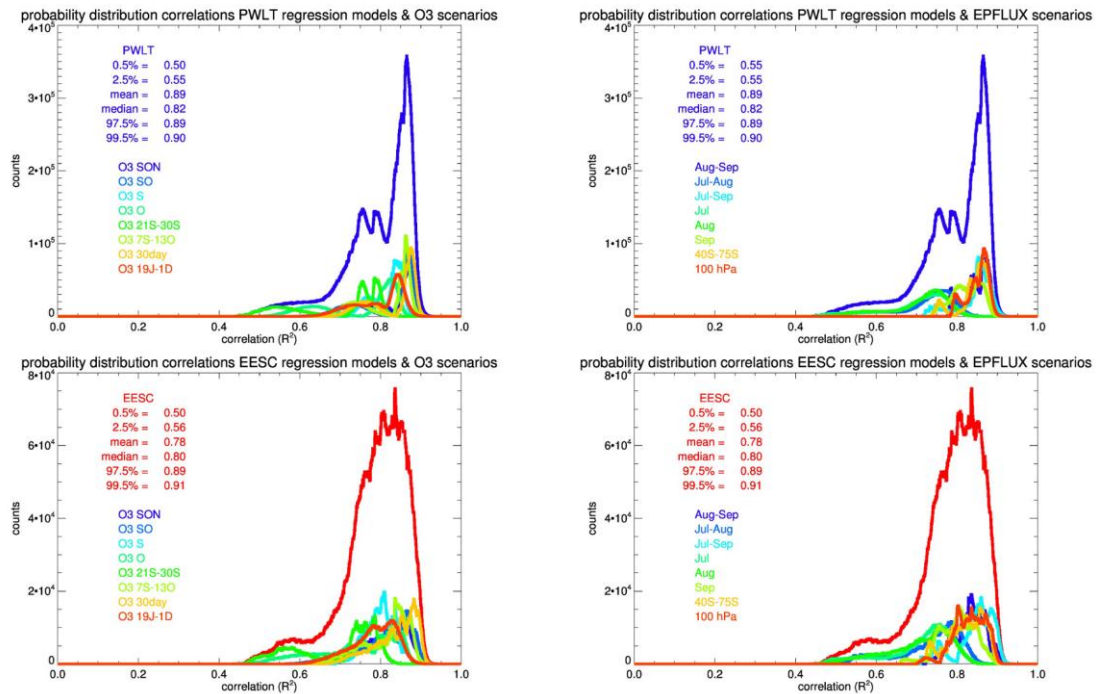


26 **Figure 3.** Time series of regressors for the period 1979-2012. For ozone, EP flux, EESC
 27 and stratospheric aerosol all scenarios as defined in section 2 are included (indicated by
 28 the different colors). For the SAM and the solar flux - QBO index only the baseline time
 29 series is shown, and both indices – being unitless to start with - are scaled for proper
 30 comparison. Ozone values are in DU, EP fluxes are in kg/s, EESC values are in ppbv and
 31 stratospheric aerosol is in optical depth.



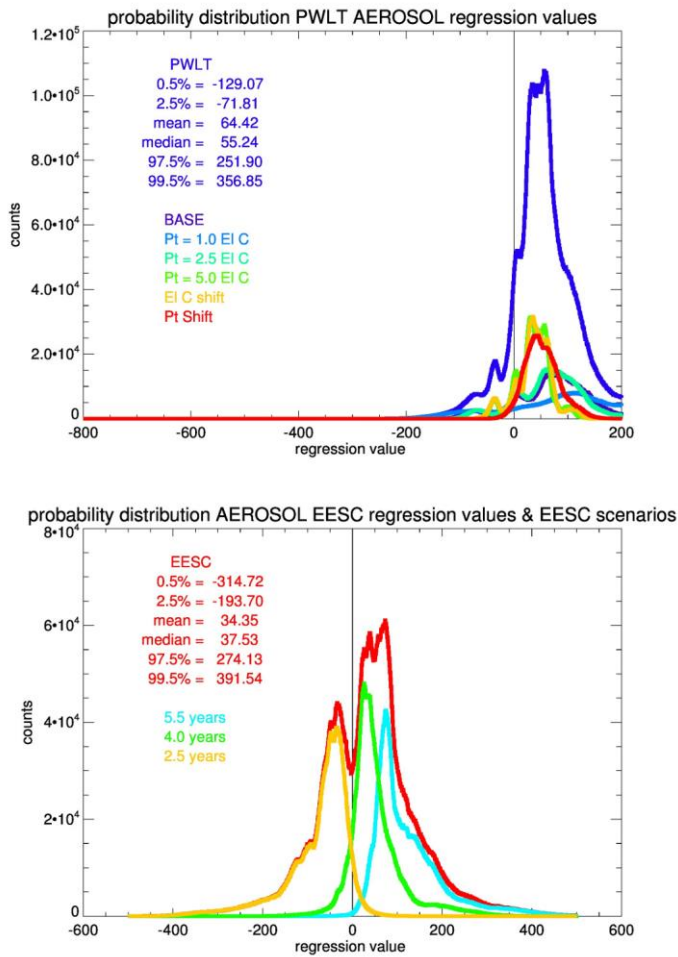
32
 33 **Figure 4.** Probability distribution of ozone trends for the period 1979-break (upper plot)
 34 and break-2010 (middle plot) as well as time correlations (R^2) for the regression models

35 and the ozone record scenarios (lower plot). The colors indicate the distributions for the
 36 two different long-term ozone regressions (EESC, PWLT). Indicated in the figure are
 37 also the 0.5%-2.5%-mean-median-97.5%-99.5% probability values of trends and
 38 correlations. The vertical black lines in the upper two panels indicate the trend (solid) and
 39 2σ errors (dotted) of the PWLT regression results of table 2 for the period 2000-2012.



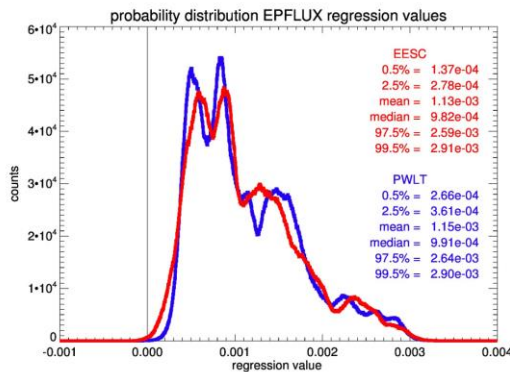
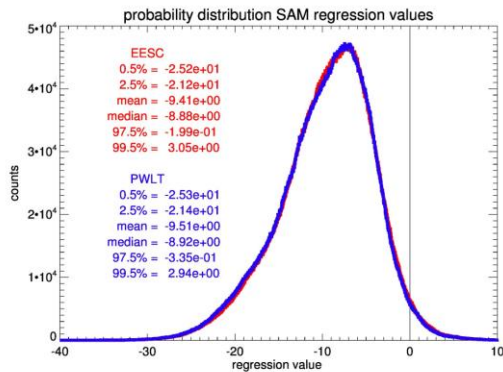
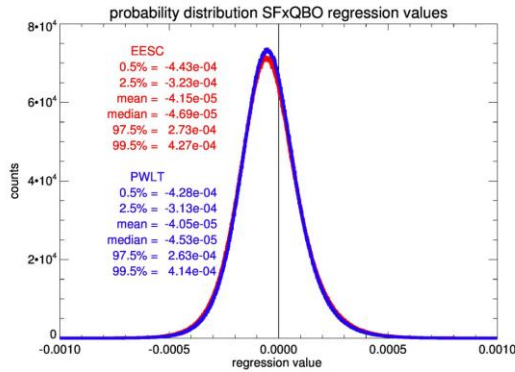
40

41 **Figure 5.** Probability distribution of regression model – ozone scenario correlations as
 42 Figure 4, lower plot, for the PWLT and EESC regression model and sensitivity to the
 43 different ozone scenarios and different EP flux scenarios, indicated by the different
 44 colors. The blue and red outlines show the sum of all scenarios combined.



45

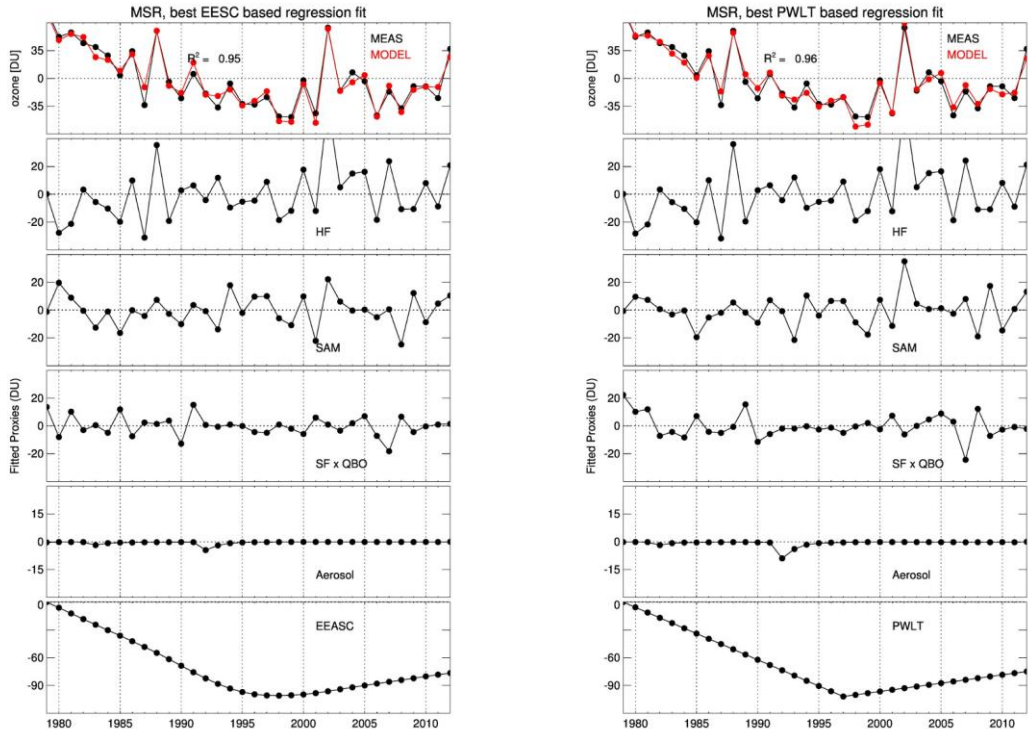
46 **Figure 6.** Upper panel: probability distribution of aerosol scenario regression coefficient
 47 values of all PWLT regression results. Included are also the distributions for the different
 48 stratospheric aerosol scenarios, indicated by the different colors. Lower panel: probability
 49 distribution of the aerosol regression coefficient values of the EESC regression model
 50 results. Included are also the distributions for the three different EESC age of air
 51 scenarios, indicated by the different colors. The blue and red outlines show the sum of all
 52 scenarios combined.



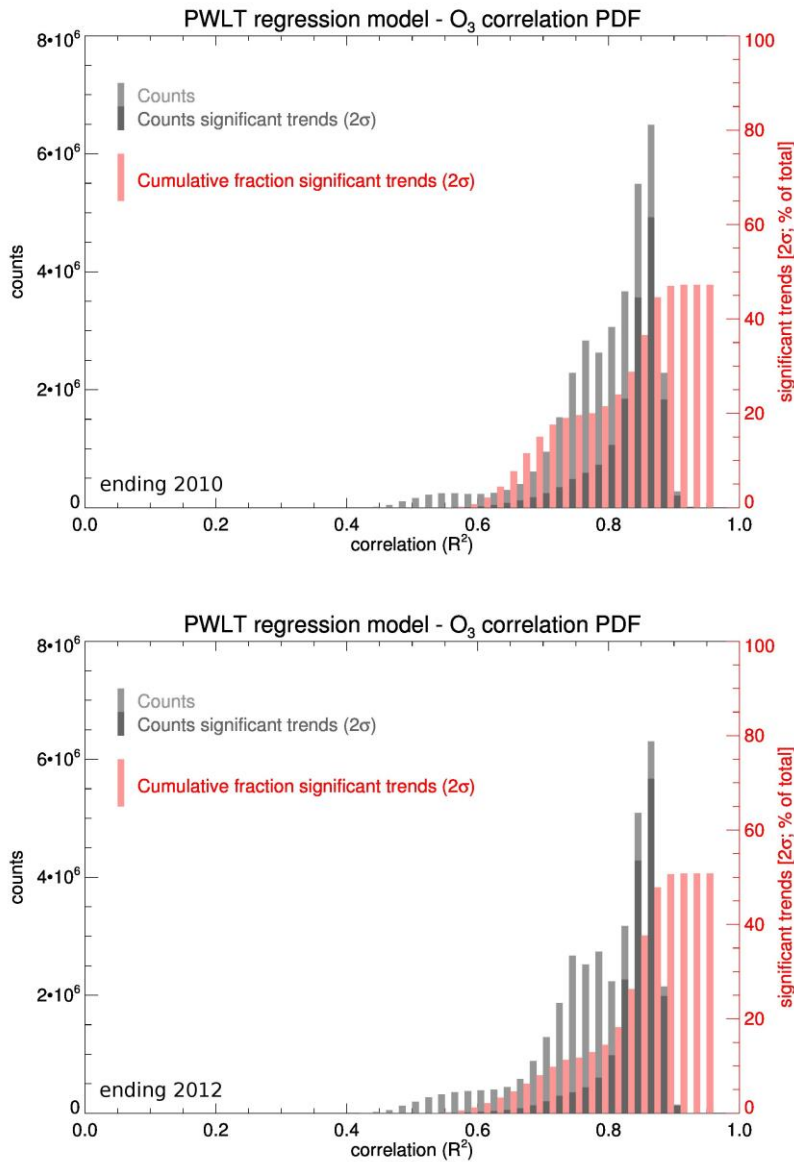
53

54 **Figure 7.** Panel A: probability distribution of the solar flux – QBO index regression
 55 coefficient values of all EESC and PWLT regression model results. Panel B: probability
 56 distribution of the SAM index regression coefficient values of all EESC and PWLT
 57 regression model results. Panel C: probability distribution of the EP flux regression
 58 coefficient values of all EESC and PWLT regression model results.

59



60
 61 **Figure 8.** Optimal regression model result for the EESC and PWLT and regressions
 62 (upper panels, red line) as well as the corresponding ozone record scenario (upper panel,
 63 black line). The ozone variations attributable to each are also shown. Ozone and ozone
 64 anomalies are given in DU.



65

66 **Figure 9.** The probability distribution of regression model – ozone record scenario
 67 correlations (R^2) as shown in Figure 5 for the PWLT regressions and the cumulative
 68 fraction of statistically significant (2σ) ozone trends for each correlation interval (red,
 69 right axis). The upper panel shows the distribution for the regressions ending in 2010, the
 70 lower panel for the regressions ending in 2012. See also Table 7.

71

